ANNUAL REVIEWS

Annual Review of Biophysics

Physical Principles Underlying the Complex Biology of Intracellular Phase Transitions

Jeong-Mo Choi,[1,2,3] Alex S. Holehouse,[1,2] and Rohit V. Pappu[1,2]

[1]Department of Biomedical Engineering, Washington University in St. Louis, St. Louis, Missouri, 63130, USA; email: jeongmochoi@kaist.ac.kr, alex.holehouse@wustl.edu, pappu@wustl.edu

[2]Center for Science & Engineering of Living Systems (CSELS), Washington University in St. Louis, St. Louis, Missouri, 63130, USA

[3]Natural Science Research Institute, Korea Advanced Institute of Science and Technology (KAIST), Yuseong-gu, Daejeon 34141, Republic of Korea

Annu. Rev. Biophys. 2020. 49:107–33

First published as a Review in Advance on January 31, 2020

The *Annual Review of Biophysics* is online at biophys.annualreviews.org

https://doi.org/10.1146/annurev-biophys-121219-081629

Keywords

phase separation, phase transition, biomolecular condensates, stickers and spacers

Abstract

Many biomolecular condensates appear to form via spontaneous or driven processes that have the hallmarks of intracellular phase transitions. This suggests that a common underlying physical framework might govern the formation of functionally and compositionally unrelated biomolecular condensates. In this review, we summarize recent work that leverages a stickers-and-spacers framework adapted from the field of associative polymers for understanding how multivalent protein and RNA molecules drive phase transitions that give rise to biomolecular condensates. We discuss how the valence of stickers impacts the driving forces for condensate formation and elaborate on how stickers can be distinguished from spacers in different contexts. We touch on the impact of sticker- and spacer-mediated interactions on the rheological properties of condensates and show how the model can be mapped to known drivers of different types of biomolecular condensates.

Contents

INTRODUCTION

Spatial and temporal organization of cellular matter determines the regulation and control of key cellular processes that lead to nontrivial outcomes such as cell division, differentiation, adhesion, motility, stress response, metabolic control, and death (19, 34, 74, 85, 98, 125, 138). Cellular matter can be organized into membrane-bound or membraneless organelles. The latter are biomolecular condensates, which are defined as concentrated nonstoichiometric assemblies of biomolecules (12), that can form via spontaneous or driven processes sharing many of the hallmarks of phase transitions (17, 154).

In 1995, Walter & Brooks (168) proposed that microcompartmentalization, which refers to the spatial organization of cellular matter, might arise due to phase separation mediated by macromolecular crowding in the cytoplasm. A generalization of this idea reemerged following the work of Brangwynne et al. (29), who showed that P-granules in germ cells form via phase separation. Since then, there has been a surge of interest in the phenomenon of liquid–liquid phase separation (LLPS), whereby biomolecular condensates form by spontaneous or driven phase separation of macromolecular components from their liquid-like environments into distinct condensates with liquid-like properties (1–11, 14, 17, 18, 20, 21, 23–25, 27, 28, 30–32, 36, 37, 39, 40, 44, 46–52, 54, 55, 57, 60–63, 67–69, 71, 72, 77–80, 83, 84, 86–90, 92, 93, 95–97, 100–102, 104, 106–109, 111–121, 123, 126, 127, 130, 133, 135–137, 139, 145, 146, 149, 150, 152, 153, 155, 157, 159–162, 164, 169–177, 179, 180, 182–184, 186) (**Figure 1**). The resulting condensates, enriched in specific macromolecules, coexist with the surrounding milieu, which is relatively deficient in the macromolecules of interest. Indeed, there is growing consensus that many membraneless biomolecular

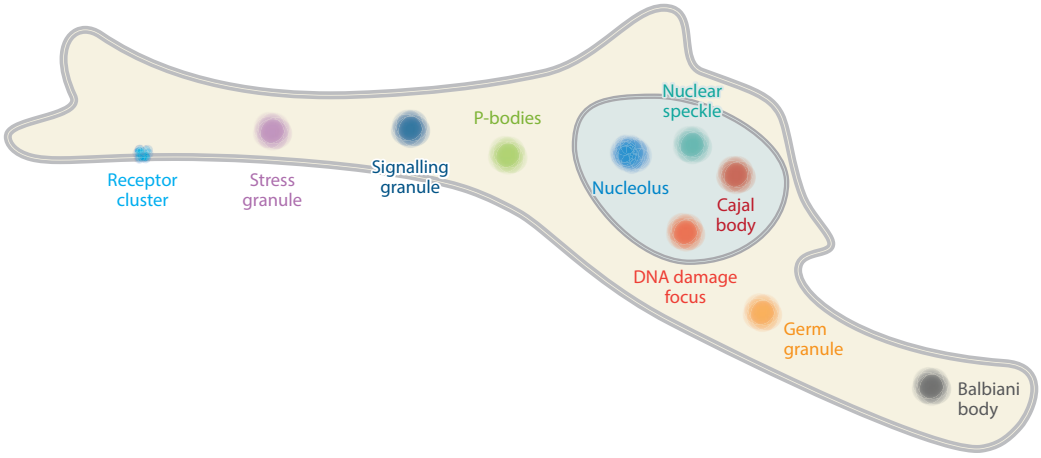

Figure 1

Overview of cellular bodies that are well described as biomolecular condensates. These bodies include large, well-studied structures such as the nucleolus, nuclear speckles, and P-bodies, but also smaller assemblies including signalling granules, receptor clusters, and DNA damage foci. The sizes of assemblies in this schematic are not to scale.

condensates form via some combination of spontaneous or driven phase separation and percolation (17, 76). Specific types of protein and RNA molecules drive intracellular phase transitions, and a defining characteristic of these molecules is the multivalence of interaction domains or motifs (12).

Phase separation, especially LLPS, is described using an assortment of analogies to observations made in everyday life. In a two-component system comprising liquids such as oil and water, phase separation is a demixing process whereby two mutually immiscible liquids form two distinct coexisting phases. Alternatively, a mixture comprising a water-soluble polymer in an aqueous solvent can separate into a dense polymer-rich phase that coexists with a dilute, polymer-deficient phase. In two-component systems comprising polymer and solvent, we use ϕ_p and ϕ_s to denote the volume fractions of polymer and solvent, respectively. If the system is closed, then $\phi_p + \phi_s = 1$, and it follows that $\phi_s = (1 - \phi_p)$; accordingly, if we set ϕ_p to be ϕ, then the volume fraction of the polymer becomes the order parameter for describing phase separation. Because the system is closed, ϕ is referred to as a conserved order parameter.

Concepts of Solvent Quality and Findings from Mean-Field Theories

In a binary mixture comprising a polymer and poor solvent, there exists a system-specific concentration threshold designated as the saturation concentration or ϕ_{sat} (31, 38, 124) beyond which the system separates into a dense polymer-rich phase that coexists with a dilute phase. The volume fractions of the polymer in the coexisting dense and dilute phases are designated as ϕ_{dilute} and ϕ_{dense}, respectively, where $\phi_{dilute} = \phi_{sat}$. For $\phi_{dilute} < \phi < \phi_{dense}$, the numbers of the polymer molecules in the two phases are determined by the so-called lever rule: $n_{dilute} = n_{total}\ (\phi_{dense} - \phi)/(\phi_{dense} - \phi_{dilute})$ and $n_{dense} = n_{total}\ (\phi - \phi_{dilute})/(\phi_{dense} - \phi_{dilute})$, where n_{dilute} and n_{dense} are, respectively, the numbers of polymer molecules in the dilute and dense phases, and n_{total} is the total number of polymer molecules: $n_{total} = n_{dilute} + n_{dense}$ (142).

In mean-field theories for homopolymer solutions, the length (N) of the polymer and the magnitude of the Flory interaction parameter χ_{ps}, which is positive in a poor solvent (59), will

determine the values of ϕ_{dense} and ϕ_{dilute}. The parameter χ_{ps} is defined as

$$\chi_{ps} = \frac{z(2u_{ps} - u_{pp} - u_{ss})}{2k_B T}. \quad 1.$$

In Equation 1, the terms u_{xy} refer to mean-field energies for interactions between species x and y; the subscripts p and s refer to the polymer and solvent, respectively. The algebraic sum of energies is made dimensionless by normalization using the parameter $k_B T$, which quantifies the thermal energy at temperature T; z is a coordination number that represents the average number of nearest-neighbor interactions that each monomeric unit within the polymer can make.

In a good solvent, χ_{ps} is negative, implying that polymer–solvent interactions are favored over polymer–polymer interactions. As a result, a homogeneous, one-phase mixture is preferred, irrespective of the value of ϕ. Conversely, χ_{ps} is positive in a poor solvent, reflecting the fact that polymer–polymer interactions are favored over polymer–solvent interactions. In a poor solvent, there exists a χ_{ps}-dependent threshold value of ϕ beyond which the system separates into two coexisting phases; this threshold value is designated as ϕ_{sat}. In a theta solvent, also known as an indifferent solvent, $\chi_{ps} = 0$, and the polymer–solvent, polymer–polymer, and solvent–solvent interactions are perfectly counterbalanced. Accordingly, the entropy of mixing is the only relevant term, and this favors the formation of an ideal, one-phase mixture in a theta solvent.

For closed multicomponent systems that comprise n types of homopolymers plus a solvent, the relevant conserved order parameter is a vector denoted as $[\phi_1, \phi_2 \ldots \phi_n]$; in this case, ϕ_i denotes the volume fraction of the polymer of type i. In a closed system, the volume fraction of the solvent is readily calculated using $\phi_s = 1 - \sum_{i=1}^{n} \phi_i$. For fixed temperature and pressure, the Gibbs phase rule prescribes that there can be a maximum of $n + 1$ coexisting phases. The determinants of the phase behavior of mixtures comprising multiple types of homopolymers plus a solvent are components of the vector $\bar{\chi} = [\chi_{12}, \chi_{13}, \ldots, \chi_{1s}, \chi_{23}, \ldots, \chi_{ns}]$, where each χ_{ij} is defined as in Equation 1; the numeric subscripts correspond to the identities of polymers, and the subscript s denotes the solvent. The main upshot is that, for aqueous mixtures of homopolymers, the mapping of phase boundaries will require knowledge of the components of the vector $\bar{\chi}$ through either numerical calculations or suitable measurements (99).

The above discussion is inspired by the influential theories of Flory and Huggins (for a discussion, see 142), and it relies on a purely mean-field description for homopolymers. The vector $\bar{\chi}$ contains all of the information that is relevant for describing the driving forces for phase separation. It is a measure of solvent quality and the mutual (in)compatibilities of polymers with one another. The compositions of dense phases and the interfacial tensions between pairs of coexisting phases are determined directly by the values of the components in the vector $\bar{\chi}$. For homopolymers, all interactions are equivalent, and $\bar{\chi}$ can be used to capture the interplay of polymer and solvent interactions to describe phase behavior.

Going Beyond Homopolymers

Homopolymers are poor approximations of most of the protein and RNA molecules that are drivers of intracellular phase transitions. These molecules are finite-sized heteropolymers of precise molecular weights that comprise structured domains and motifs, intrinsically disordered regions (IDRs), or some combination of the two. The vector $\bar{\chi}$ captures neither the sequence and structural heterogeneities nor the hierarchy of anisotropic interactions encoded by the multiway interplay among heteropolymers and the solvent. Therefore, motivated by modern developments in polymer theories, we propose that protein and RNA molecules that drive intracellular phase transitions are in fact biological instantiations of associative polymers, which were defined by

Rubinstein & Dobrynin (143, p. 181) to be "macromolecules with attractive groups." The attractive groups are distributed across the polymer. Furthermore, the interactions involving these groups can be anisotropic; these interactions include ionic bonds, hydrogen bonds, and interactions mediated by solvents known as gluonic and regulatory solvents (156).

In much the same way that the Flory-Huggins theory provides a general framework for describing homopolymeric systems, associative polymers can be described using a stickers-and-spacers model, where the mean-field free energy term from the Flory-Huggins theory is augmented by specific interactions among stickers. The groups that participate in attractive interactions are considered to be stickers, and the parts of the chain that are interspersed between stickers but do not significantly drive attractive interactions are considered to be spacers. Noncovalent interactions between stickers within and from different chains will lead to the formation of reversible physical crosslinks (143). Although spacers are not directly involved in these crosslinks, they can have a profound impact on the assembly of associative polymers.

Multivalent protein and RNA molecules may be either branched or linear associative polymers. Therefore, an important question in applying the stickers-and-spacers model to biopolymers pertains to the molecular identities of stickers. In IDRs, stickers are likely to be short linear motifs (SLiMs) that are 1–10 residues in length, while spacers are the intervening residues in the IDR (43). Analogously, in unfolded RNA molecules, stickers may be short sequence motifs or even individual nucleotides. Stickers in folded protein domains or structured regions of RNA are surface patches or motifs that emerge from the formation of specific structures. Accordingly, non-sticker regions on the surfaces of folded domains of proteins and disordered loop regions can be considered as spacers. In linear multivalent systems, stickers may be folded binding domains, while spacers are the flexible disordered linkers that connect them together. For branched multivalent proteins, disordered regions give these systems a hairy colloidal architecture, and the disordered regions, sans the SLiMs, may be thought of as spacers. **Figure 2** shows a schematic of different types of multivalent protein and RNA molecules that are mapped onto sticker-and-spacer architectures.

Importantly, the stickers-and-spacers model does not have restrictions on either the identity of stickers or the resolution at which stickers are defined. Accordingly, the stickers-and-spacers model offers an intuitive and highly generalizable approach for quantitative descriptions of complex biological systems. In the following sections, we discuss key details of the stickers-and-spacers formalism for obtaining a thermodynamic description of the phase behavior of associative polymers in solution. We summarize predictions that can be made using this model, cite numerical instantiations of the model, and highlight applications to specific protein and RNA systems.

MEAN-FIELD INCARNATION OF THE STICKERS-AND-SPACERS MODEL

One possible quantitative realization of the stickers-and-spacers framework is an analytical mean-field model for associative polymers. This model rests on the simplifying assumption that the conformational preferences of individual associative polymers are similar in their dense versus dilute phases. This simplification allows us to ignore the possibility that conformational changes might lead to changes in the valence and identities of stickers.

We consider a two-component system comprising associative polymers with multiple interacting stickers interspersed by noninteracting phantom spacers. The model for spacers assumes that the interactions involving spacers (i.e., sticker–spacer, spacer–spacer, and spacer–solvent) counterbalance one another, thus making the spacer regions behave like an ideal chain. Physical crosslinks between stickers enable two types of transitions. Aided by the nature of spacers, the physical crosslinks among stickers can lead to a density transition (which is phase separation) whereby,

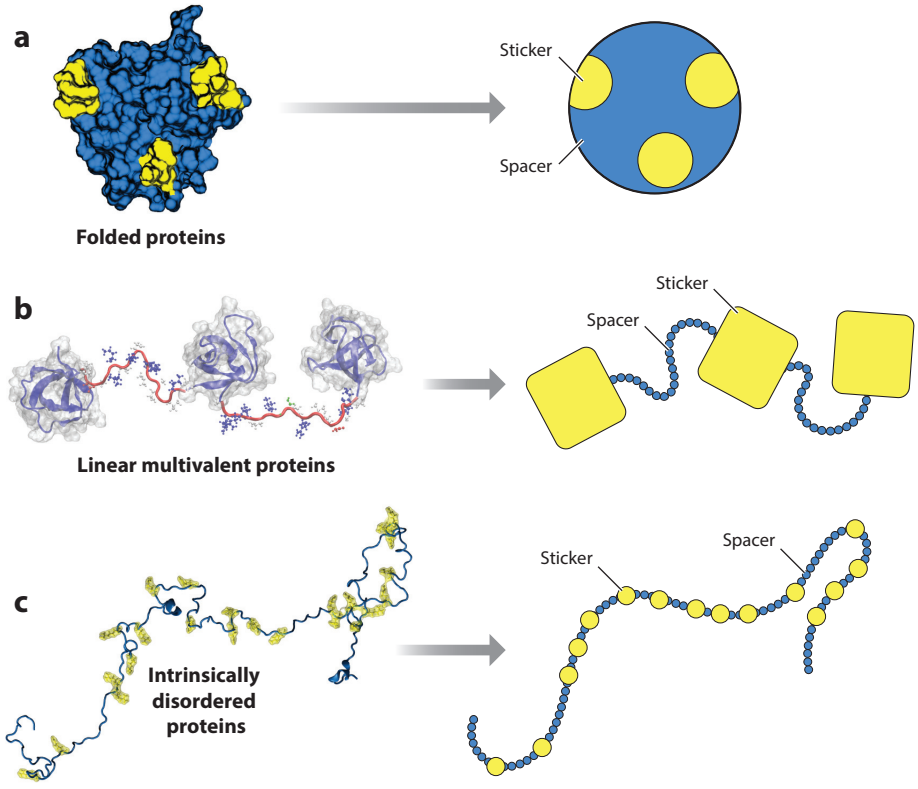

Figure 2

Schematic of different types of stickers and spacers for different systems. (*a*) For folded domains, the mapping of the stickers and spacers is achieved via the physics of patchy colloids, whereby the stickers are the interaction patches and the spacers are regions on the globular domain that serve as the surface scaffold for stickers. (*b*) For linear multivalent proteins, we can broadly map stickers as folded binding domains, while spacers are flexible linkers that connect domains. This does not rule out the prospect that disordered regions also comprise either primary or auxiliary stickers. (*c*) For intrinsically disordered proteins, stickers may be single residues, short linear motifs, or some combination of the two.

above a threshold concentration denoted as c_{sat}, the associative polymers in a binary mixture comprising the polymers and solvent will form a dense phase defined by physically crosslinked stickers that coexists with a dilute phase comprising minimal inter-sticker crosslinks. The concentrations of associative polymers or stickers in the coexisting dilute and dense phases are denoted, respectively, as $c_{dilute} = c_{sat}$ and c_{dense}. Associative polymers also undergo a networking transition known as percolation. This is governed by the topological connectivity among stickers that is engendered by physical crosslinks. Above a concentration threshold c_{perc}, known as the gel point or percolation threshold, the system of associative polymers can form a system-spanning network. Phase separation leads to percolation if $c_{sat} \leq c_{perc} < c_{dense}$. Conversely, phase separation and percolation become decoupled from one another if $c_{dense} < c_{perc}$ (phase separation without percolation) or $c_{perc} < c_{sat}$ (percolation without phase separation). For the purpose of developing the mean-field theory, we assume that we are operating in the regime where $c_{sat} \leq c_{perc} < c_{dense}$.

For a system comprising associative polymers in a solvent, each with n self-interacting stickers ($n \gg 1$), Semenov & Rubinstein (151) showed that the percolation threshold for a system in which

stickers are described as phantom chains is estimated as

$$c_{\text{perc}} \approx \frac{1}{\lambda n^2}. \qquad 2.$$

In this case, n is the apparent valence (number) of stickers, and $\lambda = v_b \exp(-\frac{\varepsilon}{k_B T})$, where v_b is the volume associated with each inter-sticker crosslink, ε is the effective interaction energy between stickers ($\varepsilon \leq 0$), k_B is the Boltzmann constant, and T is the system temperature. We describe the origins of the relationship between c_{perc} and the valence of stickers by summarizing the extension of the theory of Semenov & Rubinstein (151) to the case of an associative polymer that consists of two types of stickers, A and B.

An Obligate Heterotypic-Interaction Model for Stickers and Spacers

The theory of Semenov & Rubinstein (151) was extended by Wang et al. (170) to describe the measured variations of c_{sat} with the apparent valence (numbers) of Arg and Tyr residues that are considered to be the main stickers in FUS and FET family proteins. We follow Wang et al. (170) and assume that $\varepsilon_{\text{AA}} = \varepsilon_{\text{BB}} = 0$ and $\varepsilon_{\text{AB}} < 0$. This implies that the effective attractions arise purely from heterotypic interactions among stickers. Since $\varepsilon_{\text{AB}} < 0$, it follows that $(-\varepsilon_{\text{AB}}/k_B T) > 0$; thus, we write the Boltzmann weight as $\exp(|\varepsilon_{\text{AB}}|/k_B T)$, where the numerator of the exponent refers to the magnitude of the attractive interactions between A and B stickers.

We consider a system comprising N associative polymers in a solvent, each with n_{A} and n_{B} stickers of type A and B, respectively. The spacers between the stickers are inert, phantom chains. The free energy of the system is written as

$$\frac{F}{k_B T} = -\ln Z. \qquad 3.$$

The partition function Z can be calculated using the mean-field approach of Semenov & Rubinstein (151) as

$$Z = \Omega \exp\left(\frac{N_{\text{pairs}}\,|\varepsilon_{\text{AB}}|}{k_B T}\right)\left(\frac{v_b}{V}\right)^{N_{\text{pairs}}}. \qquad 4.$$

In Equation 4, Ω is a combinatorial factor, N_{pairs} is the total number of extant pairs of A–B crosslinks in the system, v_b is the bond volume associated with each physical crosslink, and v is the system volume. The combinatorial factor is computed as

$$\Omega = \binom{N n_{\text{A}}}{N_{\text{pairs}}}\binom{N n_{\text{B}}}{N_{\text{pairs}}} N_{\text{pairs}}!. \qquad 5.$$

Substitution of Equation 5 into Equations 4 and 3 leads to

$$\begin{aligned}\frac{F}{k_B T} = &-N n_{\text{A}} \ln(N n_{\text{A}}) + (N n_{\text{A}} - N_{\text{pairs}}) \ln(N n_{\text{A}} - N_{\text{pairs}}) \\ &- N n_{\text{B}} \ln(N n_{\text{B}}) + (N n_{\text{B}} - N_{\text{pairs}}) \ln(N n_{\text{B}} - N_{\text{pairs}}) \\ &+ N_{\text{pairs}} \ln\left(\frac{N_{\text{pairs}} V}{v_b}\right) - \left(\frac{|\varepsilon_{\text{AB}}|}{k_B T} - 1\right) N_{\text{pairs}}.\end{aligned} \qquad 6.$$

Minimizing this free energy with respect to N_{pairs} leads to

$$\frac{(N n_{\text{A}} - N_{\text{pairs}})(N n_{\text{B}} - N_{\text{pairs}})}{N_{\text{pairs}}} = \frac{V}{\lambda}. \qquad 7.$$

In this case, the attractive volume is $\lambda = v_b \exp(\frac{|\varepsilon_{AB}|}{k_B T})$. Solving the quadratic equation yields the following expression for N_{pairs} that minimizes F:

$$N_{pairs} = \frac{1}{2}\left[Nn_A + Nn_B + \frac{V}{\lambda} - \sqrt{\left(Nn_A + Nn_B + \frac{V}{\lambda}\right)^2 - 4N^2 n_A n_B}\right]. \quad 8.$$

A total of N_{pairs} stickers of type A and N_{pairs} stickers of type B will participate in N_{pairs} crosslinks. Accordingly, the fraction of interacting stickers (or crosslinks) in each chain will be

$$p = \frac{2N_{pairs}}{N(n_A + n_B)}. \quad 9.$$

Replacing N_{pairs} in Equation 8 with p leads to

$$p = \frac{1}{n_A + n_B}\left[n_A + n_B + \frac{1}{\lambda c} - \sqrt{\left(n_A + n_B + \frac{1}{\lambda c}\right)^2 - 4n_A n_B}\right]. \quad 10.$$

In this case, c is the polymer concentration N/v. If we set the strengths of sticker–sticker interactions such that $\lambda c \ll 1$ (weak interactions), then

$$p \approx \frac{2\lambda c n_A n_B}{n_A + n_B}. \quad 11.$$

Based on the Flory-Stockmayer theory (58, 158), we know that, at the percolation threshold c_{perc}, the value of p designated as p_{perc} is

$$p_{perc} = \frac{1}{n_A + n_B + 1}. \quad 12.$$

Substituting Equation 12 into the left-hand side of Equation 11 and setting $c = c_{perc}$ on the right-hand side of Equation 11 leads to the following estimate for c_{perc}, which is valid for $n_A + n_B \gg 1$:

$$c_{perc} = \frac{1}{2\lambda n_A n_B}\left(\frac{n_A + n_B}{n_A + n_B - 1}\right) \approx \frac{1}{2\lambda n_A n_B} \sim \frac{1}{n_A n_B}. \quad 13.$$

Extending the Obligate Heterotypic Model to Include Homotypic Sticker Interactions

Using a similar extension of the mean-field model developed by Prusty et al. (134), who applied the model to a system comprising distinct polymers with A and B stickers, one can include the effects of homotypic sticker attractions by setting $\varepsilon_{AA} \neq 0$ and $\varepsilon_{BB} \neq 0$. In this scenario, a generalization of the approach detailed above leads to the following expression for the percolation threshold:

$$c_{perc} \sim \frac{1}{\lambda_{AA} n_A^2 + 2\lambda_{AB} n_A n_B + \lambda_{BB} n_B^2}. \quad 14.$$

In Equation 14, λ_{ij} is the attractive volume for the i–j interaction, i.e., $\lambda_{ij} = v_{ij} \exp(\frac{|\varepsilon_{ij}|}{k_B T})$, where $\varepsilon_{ij} \leq 0$ is the interaction energy, and v_{ij} is the bond volume for the i–j interaction. Note that Equation 14 reduces to the expression in Equation 13 if the effects of homotypic interactions between stickers are ignored.

What if We Have Multiple Types of Stickers in Our System?

The model can be further generalized to a system comprising polymers with more than two types of stickers. The percolation threshold is estimated using Equation 15, written as

$$c_{\text{perc}} \sim \frac{1}{\sum_i \lambda_{ii} n_i^2 + 2\sum_{i \neq j} \lambda_{ij} n_i n_j}. \qquad 15.$$

In this case, i and j are sticker type indices, λ_{ij} is the attractive volume for the i–j interaction, and n_i is the number of stickers of type i in each polymer. As shown in Equation 15, the contribution of each sticker pair interaction is additive, weighted by the attractive volume λ_{ij}. Thus, if a certain λ_{pq} term is much greater than other terms such that the percolation concentration can be approximately evaluated by only considering $\lambda_{pq} n_p n_q$, then we can consider only stickers p and q as relevant stickers, and other stickers can be considered as spacers. This implies that there is no fixed set of stickers, and a set of stickers in one system can play the role of spacers in another system, depending on the relative contributions of different stickers to the percolation threshold.

Effects of Spacers

The preceding section builds on the work of Semenov & Rubinstein (151) and prescribes a quantitative, albeit mean-field, model for quantifying the effects of stickers on the driving forces for phase separation and percolation. One can also use the percolation threshold as a suitable proxy for estimating the saturation concentration for phase separation, providing $c_{\text{sat}} \leq c_{\text{perc}} < c_{\text{dense}}$. Whether this condition is satisfied will be determined by the nature of the spacers.

The mean-field model introduced above treats spacers as phantom chains. A simple way to account for the effects of spacers is to include ad hoc spacer-specific corrections to the average volume per crosslink, i.e., the value of v_b. However, for realistic scenarios, one has to account explicitly for the effects of spacers. There are three possible effects of spacers that one must consider: (*a*) the excluded volumes (also referred to as the effective solvation volumes) of spacers (66), which can be included using the standard Flory-Huggins formalism; (*b*) the contribution of auxiliary attractions between sites along spacers and specific stickers; and (*c*) attractive interactions between spacers that, by the definition of spacers, will be weaker than sticker–sticker interactions. In the limit of strong attractions among spacers, associative polymers essentially become akin to homopolymers in poor solvents, and the distinction between a stickers-and-spacers framework and a homopolymer model becomes minimal because all of the entities are equivalent to one another. Strong (vis-à-vis $k_B T$) sticker–sticker, sticker–spacer, and spacer–spacer interactions will drive aggregation and/or precipitation into amorphous or fibrillar solids. These assemblies are distinct from the fluid-like phases that would be formed by associative polymers. Accordingly, the excluded volumes generated by spacers and their relatively weak auxiliary interactions with stickers are the main contributions that spacers make to the phase behavior of associative polymers.

The excluded volume (v_{ex}), also referred to as the effective solvation volume (v_{es}), is the average volume per spacer site that is set aside for interactions with the surrounding volume (142) (**Figure 3*b***). It is governed by the effective, solvent-mediated, pairwise interactions between spacer sites. If these interactions are net attractive, then v_{ex} is negative, implying that the spacer sites sequester themselves from the surrounding solvent, giving rise to compact spacers. Conversely, if the effective interactions are repulsive, then v_{ex} is positive, implying that the spacer sites interact preferentially with the surrounding solvent, thereby giving rise to spacers that are conformationally expanded. If the spacer–solvent, solvent–solvent, and spacer–spacer interactions counterbalance one another, then $v_{\text{ex}} \approx 0$, implying that spacers behave like ideal chains. In theory, this

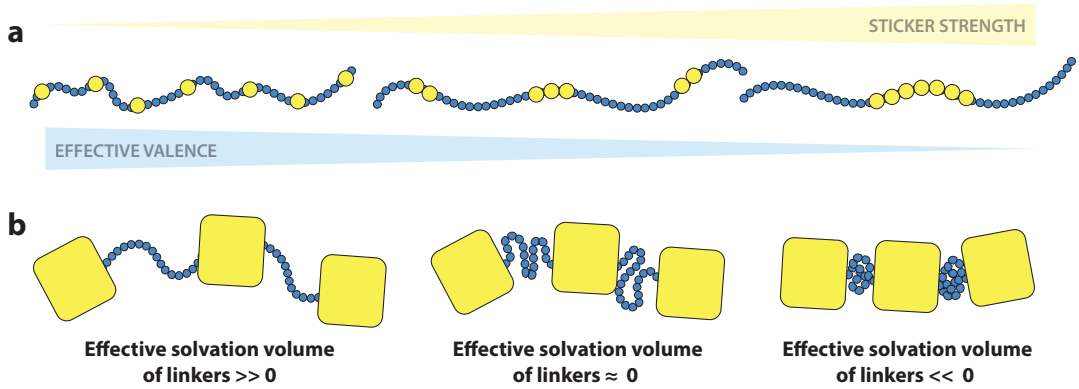

Figure 3

Schematic of sticker patterning and effective solvation volume. (*a*) Three distinct sequences of intrinsically disordered proteins with identical numbers of sticker residues distributed in different arrangements. As sticker residues are clustered together, the effective sticker identity may change such that, as the number of stickers decreases, the strength of each individual sticker increases. (*b*) Physical manifestation of the effective solvation volume (also known as the excluded volume) for linkers. A positive effective solvation volume is associated with expanded linkers, while a negative effective solvation volume leads to a collapsed and self-interacting linker. An effective solvation volume of zero derives from sequence features that give rise to counterbalanced linker–linker and linker–solvent interactions, thus engendering ideal chain behavior for the linkers.

should reproduce the mean-field behavior described above, since the mean-field model is based on so-called phantom spacers. However, the spacers with zero excluded volume can enhance the sticker–sticker interactions, and this cooperative effect leads to phase separation being realized at concentrations that are well below the percolation threshold that would be predicted based on the Flory-Stockmayer theory; this is because the Flory-Stockmayer theory only considers the valence of stickers and the bond formation probability and ignores the intrinsic connectivity due to spacers (58, 158).

Harmon et al. (66) performed lattice-based simulations intended to mimic the poly-SH3 and poly-PRM systems studied by Rosen and coworkers (15, 16, 87). Simulations showed that spacers mimicking self-avoiding walks have high positive excluded volumes, and the preferential interactions of these spacers with solvent will inhibit the cooperative interactions that are required to drive phase separation. Instead, the high excluded volumes lead to an upshift in the calculated percolation threshold when compared to expectations from the Flory-Stockmayer limit (58, 158). For associative polymers with high positive excluded volume spacers, percolation occurs above a percolation threshold, but this is realized without phase separation, implying that $c_{\mathrm{perc}} > c_{\mathrm{sat}}$ for such systems. As the spacer excluded volumes decrease, there is a stronger coupling between phase separation and percolation; this implies that the low excluded volumes of spacers enable cooperative interactions among spacers that, in turn, enable concomitant density and percolation transitions.

To account theoretically for the effects of spacers that were quantified in simulations, one has to be able to calculate the signs and magnitudes of excluded volumes for each of the spacer regions. This will allow the incorporation of suitable corrections or higher-order terms due to spacer contributions into quantitative models that allow one to predict c_{sat}, c_{perc}, and c_{dense} directly from the sequence. Continued integration between theory and simulation should permit the development of a comprehensive model that accounts for sticker valence, sticker interaction strengths, spacer excluded volumes, and higher-order contributions to interactions among associative polymers that are due to auxiliary attractive interactions between spacer sites and specific stickers.

IDENTIFYING STICKERS VERSUS SPACERS

The identification of stickers can be performed computationally and/or experimentally. As a rule of thumb, the loss of a sticker should have a substantial impact on c_{sat}, while the loss of a spacer should have minimal effects on c_{sat}. Alternatively, for multicomponent systems where the concentrations of the coexisting dilute and dense phases are not fixed quantities (see 35, figure 12), thus generalizing the concept of a saturation concentration, the rule of thumb generalizes to asking whether the loss of a sticker alters the location and slope of the coexistence curve. These are simple albeit useful zeroth-order distinctions, but quantitatively, what constitutes a substantial impact will vary across systems. A brute-force approach to identifying stickers versus spacers would be full mutagenesis of every residue using alanine or glycine scanning and/or saturation mutagenesis that is coupled with the measurements of c_{sat} for binary mixtures and/or full coexistence curves for multicomponent systems comprising each mutant. This would provide a systematic assessment of the contribution that each residue makes to the saturation concentration and/or coexistence curve, allowing those that contribute substantially to be delineated as stickers (or as falling within sticker motifs), while those that do not are delineated as spacers. In contrast, we can perform a systematic mutation of specific residues of interest, identified a priori using bioinformatics approaches (122, 166, 167, 178), to all possible amino acids. This directed saturation mutagenesis allows a direct comparison between two positions across equivalent sequence changes.

Spectroscopic Routes to Identifying Stickers Versus Spacers

Rather than assessing the functional consequence of loss (or gain) of stickers, an alternative approach is the biophysical dissection of sticker-mediated intermolecular interactions. Instead of measuring c_{sat} and/or full coexistence curves, the early stages of assembly and/or deviations from ideal solution behavior can be measured using various methods, including light scattering and fluorescence correlation spectroscopy (FCS). As an example, measuring the second virial coefficient (B_2) using laser light scattering and/or osmotic pressure measurements as a function of sequence perturbation and changes to solution conditions provides one route to dissect how distinct residues or motifs contribute to intermolecular interaction (128).

Nuclear magnetic resonance (NMR) spectroscopy is also a powerful experimental technique that provides the requisite site-specific information that can be used to identify stickers versus spacers (16, 20, 27, 164). For IDRs, transverse relaxation rates (R_2) provide information regarding local dynamics, and these may be slowed for stickers engaging in interactions with one another (105, 147). Chemical shift perturbations measured as functions of protein concentration can also provide insight into intermolecular interactions, as can cross-saturation transfer experiments. If appropriately designed experiments are performed, then paramagnetic relaxation enhancement mediated by spin labels provides an alternative approach to assess transient intermolecular interactions. Finally, if sufficiently strong intersticker interactions are present, then it may be possible to detect these using intermolecular nuclear Overhauser effects.

Many approaches used to identify stickers versus spacers will depend on the architecture of the protein and RNA molecules of interest. We define three common classes of biopolymers that fit the stickers and spacers architecture: folded domains, linear multivalent systems, and IDRs (**Figure 2**). Folded domains may be thought of as being analogous to rigid or deformable patchy colloids (117). Accordingly, the goal is to identify the attractive patches (stickers) on the surfaces of folded domains, the range and directionality of their attractions, any fluctuations associated with folded domains that may account for fluctuations between sticker–sticker interactions, and the nature of any spacer-mediated auxiliary interactions (178). A combination of computational, theoretical, and experimental approaches that have been deployed in the context of studying

the phase behavior of proteins that undergo crystallization can be adapted to identify stickers versus spacers for folded domains and quantify the interaction strengths among stickers and spacers.

The term linear multivalent proteins refers to polypeptides in which multiple folded domains are connected by flexible linker IDRs (66). Examples of such a system are the poly-SH3 + poly-PRM and the poly-SUMO + poly-SIM systems (13). For systems in which folded domains are well-defined binding modules, the stickers are readily identified as binding sites on the interaction domains (SH3 or SUMO) and their cognate partners (PRM or SIM). The relative importance of specific residues in these binding sites can be assessed by mutational studies, but auxiliary interactions mediated by residues distal from these sites may also have a modulatory role (16). In these types of modular systems, the flexible linkers that connect folded domains can be viewed as the spacers. The surface residues that lie outside the binding sites may also be viewed as auxiliary spacers. Similar approaches can be applied to branched multivalent proteins comprising folded oligomerization domains and IDRs, as in the case of nucleophosmin 1 (NPM1) (57), or even oligomeric proteins such as metabolic enzymes that are devoid of IDRs.

To identify and delineate stickers from spacers within IDRs, we can take advantage of the maturity of methods that are now routinely being brought to bear on the analysis of conformational ensembles of disordered proteins in dilute solutions. This becomes an informative exercise in the context of IDRs that lack persistent secondary or tertiary structural preferences, as there is an intrinsic equivalence between intermolecular and intramolecular interactions. Degenerate interactions, in the form of a network of intramolecular physical crosslinks among stickers along an IDR, can lead to the partial collapse of individual molecules. Two distinct types of parameters can be determined from these single-chain simulations: parameters determined from the sequence alone and the apparent valences of stickers and chain length. Additionally, one can obtain parameters that are governed by a combination of sequence and solution conditions and include the sticker–sticker interaction strengths and the excluded volumes of spacer regions. Both sets of parameters play a key role in determining the extent of collapse of an individual disordered protein in dilute solutions and, consequently, the extent of intermolecular interactions in sufficiently concentrated solutions. Accordingly, an assortment of methods that combine experimental and computational approaches can be used to identify and delineate stickers versus spacers in IDRs.

The combination of methods described for multivalent proteins can also be brought to bear on identifying stickers versus spacers in RNA molecules. These methods can be augmented by RNA structure prediction methods that help identify regions of complementarity that are likely to be involved in making secondary structures via base pairing and base stacking. Secondary and tertiary structure predictions are readily tested using methods such as selective 2′-hydroxyl acylation analyzed by primer extension (94) that are sensitive to the presence of specific types of structural motifs. Recent work has shown that the ratio of purines to pyrimidines is an important determinant of the driving forces for phase separation in disordered RNA molecules (22). This observation provides a useful heuristic to quantify comparative driving forces for phase separation on the basis of the apparent valence of purine-based stickers compared to pyrimidine-based spacers.

Apparent Valence Versus Effective Valence of Stickers

The approaches of Semenov & Rubinstein (151) focus primarily on the apparent valence of stickers. Recent studies have shown that the clustering and segregation of stickers along linear sequences can have a profound effect on the driving forces for phase separation. For a fixed number (apparent valence) of stickers, sequence patterning can increase or decrease the effective valence of

stickers (**Figure 3*a***). Coarse-grained simulations based on transferrable (46), phenomenological (35, 57), or learned models (144) have been developed and deployed to study the phase behavior of an assortment of protein and RNA molecules that include a combination of folded domains and disordered regions (65, 66, 131, 141). The results of simulations can be analyzed using mean-field theories, and discrepancies between theoretical predictions and computational results can be used to extract the effective valence of stickers, thereby going beyond the apparent valence extracted from sequence analysis alone.

An important theoretical advance that accounts for sequence patterning effects, specifically the clustering versus segregation of charged residues, comes from Chan and coworkers (91, 92). Building on observations of the contributions of charge patterning to the dimensions of disordered proteins, Lin & Chan (91) adapted the generalized random phase approximation originally introduced by Ermoshkin & Olvera de la Cruz (53) for synthetic polymers to incorporate sequence correlations among charged stickers and a mean-field correction to model cation–pi interactions. Their model has been used to predict differences in phase behavior for sequences that have identical numbers (apparent valence) of charged residues but are distinguished by the patterning of oppositely charged residues along the linear sequence (27). Their predictions reveal that the effective valence is lower than the apparent valence for sequences where the oppositely charged residues are segregated along the linear sequence, but the strength of sticker–sticker interactions increases substantially when compared to sequences with a more uniform distribution of charged stickers. In contrast, the effective valence is lower than the apparent valence for sequences where the oppositely charged residues are well mixed along the linear sequence. The predictions of Chan and coworkers have also been borne out in orthogonal field-theoretic simulations and in experiments based on synthetic polymers (103). These studies, as well as in vitro and in cell experiments aided by sequence design approaches (123), highlight the importance of sequence patterning effects as determinants of the effective valence as opposed to the apparent valence.

The apparent and effective valences can also deviate from one another if the associative polymer of interest is characterized by conformational heterogeneity. For highly structured systems and maximally disordered systems, there is likely to be a one-to-one correspondence between apparent valence and effective valence. Between these limiting scenarios, the dominant conformations in the ensembles within dilute and coexisting dense phases will govern the effective valence.

CONTRIBUTIONS OF STICKER–STICKER CROSSLINKS AND SPACER EXCLUDED VOLUMES TO STRUCTURAL AND DYNAMICAL PROPERTIES OF CONDENSATES

Condensates formed by associative polymers are not simple liquids, which are formed by spherical molecules with isotropic interactions. In contrast, liquids formed by associative polymers are characterized by physical crosslinks among highly flexible (disordered) polymers or patchy colloidal (ordered) molecules. Accordingly, these liquids are best described as network fluids (45).

The rheological properties of network fluids are governed by the extent of crosslinking, the timescales associated with making and breaking of physical crosslinks, the concentration of stickers within the dense phase, and the modulatory impact of spacers (45). Network fluids are not purely viscous liquids, but they behave like elastic materials on timescales shorter than the lifetimes of crosslinks (143). On longer timescales, these fluids behave like viscous materials, and therefore, network fluids are in fact viscoelastic rather than purely viscous fluids. Rheological characterization of viscoelastic materials requires the measurement of dynamic moduli, which quantifies the ratio of stress to strain of the fluid under the influence of oscillatory forces (141, 143). Of direct

relevance is the response of a network fluid to shear stresses and strains. If the fluid is purely viscous, then the shear strain, which refers to the deformation of the network, will lag behind the shear stress, which refers to the breaking of the network. Conversely, in a purely elastic material, the stress and strain are perfectly in phase. The phase angle between stress and strain can be quantified in terms of the dynamic modulus G^*, which is a complex variable written as $G^* = G' + iG''$. In this case, G' and G'' are the shear storage and shear loss moduli, respectively. The storage modulus quantifies the energy stored in the network and is determined by the extent of physical crosslinking and the strengths of the crosslinks. In contrast, the loss modulus quantifies the extent of energy dissipation and is governed by the viscosity of the fluid. Values of storage and loss moduli can be measured as functions of shearing frequency, and the phase angle δ is calculated as the ratio of loss to storage modulus, i.e., $\tan \delta = (G''/ G')$.

Is the Distinction Between Viscous and Viscoelastic Network Fluids Relevant or of Functional Importance?

Nucleoli (57), nuclear speckles (56), P-granules (73, 135), and even very simple synthetic condensates (22, 155) show characteristics of multilayered, multicomponent behavior (**Figure 4**). Distinct layers are likely to form via different molecular interaction networks, and these may lead to different viscoelastic behaviors. Rheological measurements show that the fibrillarin-rich dense fibrillar center (DFC) of nucleoli derived from oocytes is a bona fide viscoelastic material (57). Comparatively, the NPM1-rich granular component appears to be more of a viscous material than the DFC. Nucleoli and nuclear speckles appear to have similar organizations in that their cores are more viscoelastic than the outer layers, which are more viscous. This type of architecture might have a bearing on where and when rRNA and ribosomal proteins, which experience opposing radial fluxes in nucleoli, will encounter one another and undergo ribosomal assembly (109). In contrast to nucleoli and nuclear speckles, condensates formed by essential P-granule components such as MEG proteins and their cognate RNA molecules appear to have viscous cores surrounded by viscoelastic shells (135). Although rheological measurements are not available for this condensate, inferences were drawn using data from experiments based on fluorescence recovery after photobleaching, and these might come with requisite caveats regarding their analyses (163). The coexistence with viscous protein-like liquids and apparently viscoelastic materials comprising physically crosslinked

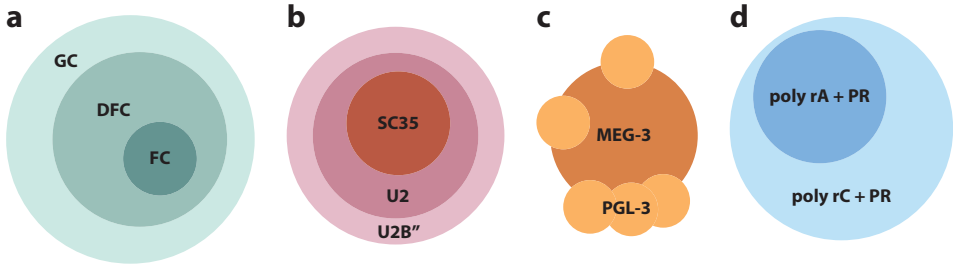

Figure 4

Four examples of multiphase assemblies formed for different multicomponent systems. (*a*) Three-phase assembly of nucleoli is readily reproduced using a simple stickers-and-spacers model, as shown by Feric et al. (57). (*b*) Distinct types of nuclear speckle architecture can also be recapitulated in a similar manner, as shown by Fei et al. (56). (*c*) MEG-3 and PGL-3 form distinct phases in P-granules and in vitro, as demonstrated by Putnam et al. (135). (*d*) A simple four-component system (solvent, proline–arginine dipeptides, polyadenosine, polycytosine) forms two distinct dense phases due to distinct sticker–sticker strengths, as described by Boeynaems et al. (22).

RNA molecules is also readily observed in binary and ternary systems with simple dipeptide-rich proteins and homopolymeric RNA molecules (22).

Connecting Dynamic Moduli to Internal Structures Within Condensates

Dynamic moduli quantify the material properties of viscoelastic network fluids, and these moduli are determined by the spatial organization of associative polymers with respect to one another within condensates. Spatial organization of molecules will also determine the crosslinking density within condensates. One can quantify spatial organization using distribution functions, such as pair and triplet distribution functions, that serve as primary descriptors of the structures of liquids. These structural descriptors, which delineate the length scales for short-range spatial order versus long-range disorder, can be augmented by descriptions of orientational distribution functions as well. The use of distribution functions completely revolutionized the studies of simple liquids and molecular fluids formed by small molecules. Building on these advances, Zwanzig & Mountain (185) derived direct connections between the structures of liquids quantified in terms of pair distribution functions and dynamic moduli for simple liquids. Extensions of these approaches to connect structural descriptions of network fluids formed by associative polymers to their dynamic moduli are precisely the types of connections between structural descriptions of condensates and their material properties that are needed to understand structure–function relationships on mesoscales defined by nonstoichiometric macromolecular assemblies. Such efforts will be aided by recent advances in small-angle neutron scattering measurements that enable the measurement of indirect Fourier transforms of pair distribution functions, as has been demonstrated by Mitrea et al. (108) for facsimiles of pentameric NPM1 that form condensates through heterotypic interactions with Arg-rich ligands.

THE STICKERS-AND-SPACERS MODEL IN BIOLOGICAL SYSTEMS

A variety of condensate-driving systems, including multivalent protein and RNA molecules, appear to conform to the stickers-and-spacers architecture. The earliest demonstration of the relevance of the stickers-and-spacers model was made by Rosen and coworkers (15, 87), who studied the phase behavior of linear multivalent proteins in solution and anchored to membranes. In accord with the predictions of Semenov & Rubinstein (151) and tenets of the Flory-Stockmayer theory, the valence of interaction domains was shown to contribute directly to the driving forces for phase separation and percolation or gelation. Furthermore, in cells, multisite Tyr phosphorylation was shown to regulate the overall valence of stickers by recruiting multiple proteins with multiple SH3 and SH2 domains to the membrane-anchored protein nephrin (87).

Associative polymers can form system-spanning networks, a phenomenon that is known as percolation. If phase separation and percolation are coupled ($c_{sat} \leq c_{perc} < c_{dense}$), then the dense phase is a percolated network. In the scenario where the dense phase is a spherical droplet, it follows that the associative polymer forms a droplet-spanning network that coexists with a dilute phase of non-networked molecules. Associative polymers can also form networked solid phases, as is the case with so-called self-assembled fibrillar networks (42). In these cases, the associative polymers form fibrillar structures—as has been observed with several low-complexity sequences—at sufficiently high concentrations. These fibrils are crosslinked to form networks that are akin to self-supporting hydrogels, and in contrast to systems that undergo LLPS through weak degenerate multivalent interactions, these systems are characterized by the acquisition of specific structural biases within the networked phase that are largely absent from polypeptides in the dilute phase.

In the context of low-complexity intrinsically disordered proteins, McKnight and coworkers (64, 75, 81, 82) identified stickers that drive the formation of cross-beta structures and enable the

networking of fibrils, thus giving rise to highly networked hydrogels. The Eisenberg group leveraged their ability to make microcrystals using peptide fragments to identify stickers that enable the formation of intermolecular crosslinks in the form of hydrogen bonds and zippering interactions. In their parlance, Eisenberg and coworkers (70) refer to the stickers as LARKS (low-complexity aromatic-rich kinked segments) due to their sequence composition and the fact that they form cross-beta structures with a characteristic kinked topology, in contrast to standard amyloid cross-beta regions.

Brangwynne et al. (31) proposed that stickers in disordered regions were likely to be SLiMs made up of charged, polar, and aromatic moieties. Drawing on the decades-old work of Burley & Petsko (33), Brangwynne et al. proposed that the three categories of residues were likely to be involved in a hierarchy of weakly polar interactions due to their intrinsic multipole moments. Charged residues such as Arg are defined by a monopole moment (charge of $+1e$), a finite dipole moment, and a significant quadrupole moment due to the planarity of the guanido group. In contrast, Lys has a spherically symmetric functional group and is better approximated as a point charge with a monopole moment (charge of $+1e$) but a negligible dipole or quadrupole moment. This would imply that Arg would be a superior sticker residue over Lys given the hierarchy of interactions that it encodes. In accord with this expectation, Wang et al. (170) showed that the network of Arg–Tyr interactions derived from the high valence of Arg residues within the RNA binding domain (RBD) and equally high valence of Tyr residues within the prion-like domain (PLD) contributes directly to the driving forces for phase separation of the protein FUS. Mutations of Arg to Lys within the RBD weaken the driving forces by approximately tenfold, as measured by the impact of these mutations on the value of c_{sat}. Tyr residues have zero net charge (zero monopole moment) but a large dipole moment, due to the in-plane arrangement of the –OH group with the planar pi system, and a significant quadrupole moment that is in accord with its aromaticity. In contrast, Phe has a near-zero dipole moment and a finite quadrupole moment that is concordant with that of Tyr. Accordingly, substitution of the Tyr residues within the PLD of FUS with Phe residues causes a diminution of the driving forces for phase separation, measured again in terms of increased values for c_{sat}. The roles of hydrophobic stickers have been made clear in the work of Riback et al. (139), who quantified the effects of titrating hydrophobic residues on the driving forces for collapse and phase separation of the polyA RNA binding protein PAB1.

Recent work of Castañeda and coworkers (41, 181) has shown the validity of the distinctions between stickers and spacers for explaining the impact of amyotrophic lateral sclerosis–related mutations within the protein UBQLN2 on its phase behavior. Mutations to stickers alter the driving forces for phase separation, whereas mutations to spacer residues contribute to changes in molecular dynamics as measured by the recovery of fluorescence after photobleaching. Interestingly, mutations to spacer residues have minimal effects on the driving forces for phase separation, a result that is concordant with the observations of Wang et al. (170), who found that changes to the PLD and RBD of FUS that lie outside of the identified stickers (Tyr and Arg) impact the material properties of condensates without altering the driving forces for phase separation.

The impact of charged residues as stickers was explored in the DEAD box helicase protein DDX4, which drives the formation of nuage bodies. Nott et al. (121) were the first to show the importance of clusters of positively and negatively charged residues along the linear sequence, with modest sequence changes that disrupt these charged stickers preventing phase separation in cells through a reduction in valence without changing sequence composition. They were also the first to identify the importance of complementary interactions between cationic and Phe (aromatic) residues as drivers of phase separation. The importance of linear clustering of charged stickers was also uncovered by Pak et al. (123), who quantified the phase behavior of a de novo designed IDR, the nephrin intracellular domain (NICD), in cells and in vitro, showing that increased linear

clustering of acidic residues within NICD enhances the driving forces for phase separation and the extent of physical crosslinking aided by cationic complexing polyions. As for RNA molecules, mutagenesis studies, design experiments, and coarse-grained simulations have demonstrated that purines are stronger stickers than pyrimidines, a result attributed to their double ring structure, which gives rise to a stronger aromatic system (22).

EMERGENT VERSUS INTRINSIC STICKERS

Instantiations of the stickers-and-spacers model summarized above have focused on sequence-encoded features that dictate the apparent and effective valence of stickers. These stickers are intrinsic to the molecular architecture and are directly encoded into the sequence. Thus, we refer to these as intrinsic stickers. Recently, it has become clear that hierarchical assembly processes can give rise to emergent stickers, in which oligomerization and clustering or even microphase separation (141) can give rise to a de novo multivalent macromolecule that is itself able to drive the formation of condensates via the types of interactions that are proposed to apply for associative polymers (**Figure 5*a***). Clusters that serve as generators of emergent stickers can form at a relatively low molecular concentration compared with the saturation concentration associated with their constitutive monomeric components. Importantly, from a theoretical standpoint, it can be argued that the interactions that drive oligomerization and clustering are likely to be distinct from the interactions that drive coalescence of oligomers into condensates, the conversion of clusters into crystals (165), or the transformation of oligomers into fibrils (131, 148).

We highlight several concrete examples that anchor the idea of emergent stickers being generated from oligomers or clusters. A subset of auxin response transcription factors (ARFs) in *Arabidopsis thaliana* undergo oligomerization driven by a folded C-terminal, PB1 (132). These linear oligomers lead to the formation of higher-order species, which themselves drive the formation of condensates through an IDR-dependent assembly process. In this system, oligomerized ARFs are in effect large multivalent biopolymers that drive condensate formation through the crosslinking of stickers in IDRs, whose multivalence is governed by the extent of oligomerization. If PB1 oligomerization is abrogated though a single lysine-to-alanine mutation, then higher-order oligomers and, consequently, condensates are unable to form (**Figure 5*b***). As a second example, in the NPM1 pentamer, an emergent molecular species undergoes phase separation, as opposed to NPM1 monomers individually (108–111). A third example is the SPOP system, which has been explored in a series of elegant experiments (25, 101, 129). Finally, dimerization of HP1a/α plays a key role in forming a species with the requisite multivalence to undergo phase separation (84, 159). A synthetic system where oligomerization controls the valence of IDRs that drive condensate formation is the Corelet system designed by Bracha et al. (26). In this case, the valence of IDRs appended to the oligomeric ferritin core is controlled by light, and the driving forces for phase separation, as quantified by full coexistence curves measured in living cells, are governed by the valence of the IDRs. In all of these systems, oligomerization that leads to emergent multivalence of stickers involves either evolved or designed interactions that are clearly orthogonal to the interactions that drive condensate formation through multivalence of stickers in IDRs.

A simple rationalization for the benefit of oligomerization and clustering is that they help to prepay some of the entropic penalty, a feature that can only be truly realized if the modes of interaction that drive oligomerization and subsequent condensate formation are distinct. This condition is well aligned with the observation that many of the proteins that undergo phase separation possess a modular architecture with distinct interaction domains (both IDRs and folded binding domains). The existence of orthogonal modes of intermolecular interaction allows the driving force for assembly to be tuned at (at least) two independent and complementary sites (**Figure 5*c***).

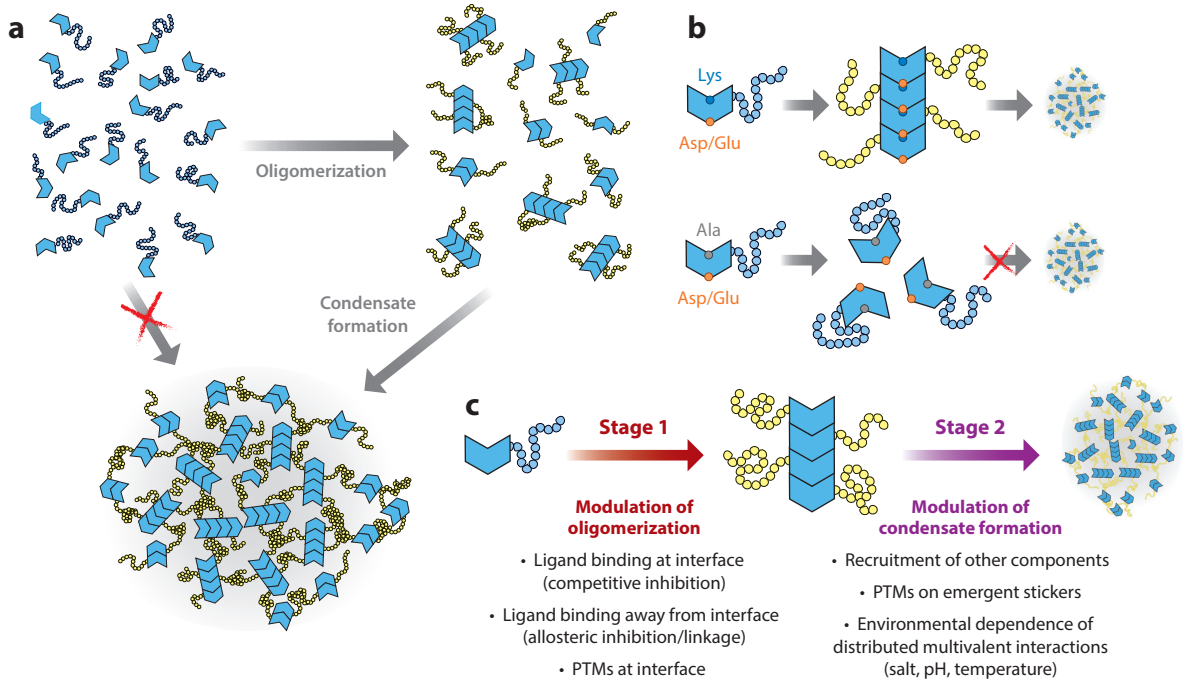

Figure 5

General model for emergent stickers formed through oligomerization, linear polymerization, and/or clustering. (*a*) Depiction of monomers of ARF19 (*solid shapes*) that correspond to the PB1 domain and the disordered low-complexity prion-like domain shown as a string of smaller blue spheres tethered to the PB1 domain. Monomers lack the requisite valence to drive condensate formation, but oligomerization gives rise to polymers with emergent multivalence of IDRs (*yellow*). Polymers of ARF19 can drive condensate formation through physical crosslinking among IDRs. (*b*) ARF19 molecules undergo spontaneous polymerization through electrostatic interactions that are mediated via complementary interfaces involving the PB1 domain. Neutralization of a lysine residue abrogates polymerization and this in turn prevents condensate formation. (*c*) Schematic that summarizes the modus operandi for condensate formation through crosslinks among emergent stickers that result from oligomerization, polymerization, and/or cluster formation. For a system that gives rise to emergent stickers, condensate formation can be regulated at two levels: In stage 1, an effectively binary regulation that dictates whether oligomerization occurs (modulation of valence), and in stage 2, a second level in which the strength of emergent stickers can be altered. Note that, temporally, the order in which these levels of modulation occur is irrelevant. As a tangible example, in a scenario in which IDR phosphorylation weakens the strength of emergent stickers, the act of phosphorylation could happen before or after oligomerization. The binding of ligands, which could include other proteins, nucleic acids, or small molecules, either may lead to a conformational transition that allows homotypic oligomerization or could itself drive heterotypic assembly. In principle, multiple nested layers of assembly via orthogonal interaction modes provide the foundations for arbitrarily complex regulation. Abbreviations: IDR, intrinsically disordered region; PTM, post-translational modification.

From a regulatory standpoint, this allows one set of regulatory systems to control on–off interactions (e.g., inhibition or promotion of oligomerization or clustering) and another to tune the molecular details of the condensate by modulating the strength of emergent stickers. While we describe oligomerization in this review in terms of a conventional and stoichiometric biochemical phenomenon (i.e., dimerization, polymerization, etc.), oligomerization could also itself be driven by weak multivalent interactions, which would necessarily be chemically orthogonal to those that drive higher-order assembly. The multiresolution nature of the stickers-and-spacers model is appealing, as the emergence of new stickers is well described as a fractal (self-similar) phenomenon, allowing the same theoretical framework to be quantitatively applied irrespective of the molecular nature and length scale.

CONCLUDING REMARKS

The field of intracellular phase transitions is evolving rapidly as we learn more about the molecular drivers of biomolecular condensates and the contributions of condensates to specific biological functions. Condensates appear to be ubiquitous within cells, and novel cellular functions are being ascribed to newly discovered condensates. Accounts of these novel functions and details about the molecular drivers of condensates are emerging at a frenetic pace. In this review, we focus on a specific physical framework, namely, the stickers-and-spacers model, adapted from the field of associative polymers, to describe the molecular grammar that underlies the architecture, sequence-encoded driving forces, and evolution of the multivalent protein and RNA molecules that drive condensate formation. Mapping of the stickers-and-spacers framework to biomacromolecules is in its infancy. However, the validity of this framework is coming into sharp focus as more accounts emerge of its utility for explaining measured phase behavior and for predicting and designing phase behavior. The availability of computational tools is further advancing our ability to dissect the interplay between spontaneous and driven processes in regulating and determining the phase behavior of mixtures of associative polymers. At this juncture, the stickers-and-spacers formalism seems like an apt modernization of classical theories developed for homopolymers and is proving to be relevant for describing phase transitions of multivalent protein and RNA molecules. The findings summarized in this review pave the way for understanding how the synergies of sticker and spacer interactions might be affected or modulated in multicomponent systems, which mimic naturally occurring biomolecular condensates—an important topic that merits intense study.

Predictions based on the stickers-and-spacers framework apply to systems with one or two types of multivalent protein or RNA molecules in a solvent. However, biomolecular condensates encompass hundreds of distinct types of macromolecules. A key concept that has to be generalized is that of saturation concentrations, as what we have adapted thus far applies strictly to two-component systems comprising a polymer plus a solvent. A recent computational study based on the LASSI simulation engine helps generalize the concept of saturation concentration by showing how obligate heterotypic interactions can give rise to apparent saturation concentrations that depend on the slopes of tie lines in multidimensional phase diagrams (35). The simulations, which are built on the stickers-and-spacers formalism, when combined with suitable experiments (140), should enable a rigorous mapping between the numbers of distinct components and the apparent saturation concentrations for each of the components. In fact, our generalizations of c_{perc} (see Equation 15) for an arbitrary number of stickers, as well as the findings reported by Choi et al. (35) based on the LASSI engine and by Riback et al. (140) based on experiments, help set the stage for connecting generalized observations from simulations of multicomponent systems to theories wherein each protein or RNA component has its own set of distinct stickers that may or may not interact with stickers on other protein or RNA molecules.

DISCLOSURE STATEMENT

R.V.P. is a member of the Scientific Advisory Board of Dewpoint Therapeutics, Inc. This membership has not influenced the scientific content of this review. The other authors are not aware of any affiliations, memberships, funding, or financial holdings that might be perceived as affecting the objectivity of this review.

ACKNOWLEDGMENTS

The US National Science Foundation (MCB-1614766), the US National Institutes of Health (5R01NS056114 and 1R01NS089932), the Human Frontier Science Program (RGP0034/2017),

and the St. Jude Research Collaborative on Membraneless Organelles fund ongoing efforts in the Pappu lab. J.-M.C. is currently funded by the Basic Science Research Program (2019R1A6A1A10073887) from the Ministry of Education of the Republic of Korea through the National Research Foundation of Korea. We are grateful to Simon Alberti, Priya Banerjee, Clifford Brangwynne, Carlos Castãneda, Hue-Sun Chan, Furqan Dar, Julie Forman-Kay, Titus Franzmann, Amy Gladfelter, Tyler Harmon, Anthony Hyman, Frank Jülicher, Richard Kriwacki, Erik Martin, Tanja Mittag, Ammon Posey, Michael Rosen, Lucia Strader, Andrea Soranno, and J. Paul Taylor for numerous stimulating discussions. We dedicate this review to the memory of Suzanne Eaton, a senior group leader at the Max Planck Institute for Cell Biology (MPI-CBG) and Genetics in Dresden, where the application of the stickers-and-spacers formalism matured through interactions with colleagues at the MPI. Suzanne was an inspiring scientist and human being, and her legacy will continue to live on through the efforts of scientists at the MPI-CBG and the community that stretches beyond.

LITERATURE CITED

1. Abbondanzieri EA, Meyer AS. 2019. More than just a phase: the search for membraneless organelles in the bacterial cytoplasm. *Curr. Genet.* 65:691–94
2. Aguzzi A, Altmeyer M. 2016. Phase separation: linking cellular compartmentalization to disease. *Trends Cell Biol.* 26:547–58
3. Alberti S. 2017. Phase separation in biology. *Curr. Biol.* 27:R1097–102
4. Alberti S, Gladfelter A, Mittag T. 2019. Considerations and challenges in studying liquid-liquid phase separation and biomolecular condensates. *Cell* 176:419–34
5. Alberti S, Saha S, Woodruff JB, Franzmann TM, Wang J, Hyman AA. 2018. A user's guide for phase separation assays with purified proteins. *J. Mol. Biol.* 430:4806–20
6. Alexander EJ, Ghanbari Niaki A, Zhang T, Sarkar J, Liu Y, et al. 2018. Ubiquilin 2 modulates ALS/FTD-linked FUS–RNA complex dynamics and stress granule formation. *PNAS* 115:E11485–94
7. Al-Husini N, Tomares DT, Bitar O, Childers WS, Schrader JM. 2018. α-Proteobacterial RNA degradosomes assemble liquid-liquid phase-separated RNP bodies. *Mol. Cell* 71:1027–39.e14
8. Altmeyer M, Neelsen KJ, Teloni F, Pozdnyakova I, Pellegrino S, et al. 2015. Liquid demixing of intrinsically disordered proteins is seeded by poly(ADP-ribose). *Nat. Commun.* 6:8088
9. Amaya J, Ryan VH, Fawzi NL. 2018. The SH3 domain of Fyn kinase interacts with and induces liquid-liquid phase separation of the low-complexity domain of hnRNPA2. *J. Biol. Chem.* 293:19522–31
10. Aumiller WM Jr., Keating CD. 2016. Phosphorylation-mediated RNA/peptide complex coacervation as a model for intracellular liquid organelles. *Nat. Chem.* 8:129–37
11. Aumiller WM Jr., Keating CD. 2017. Experimental models for dynamic compartmentalization of biomolecules in liquid organelles: reversible formation and partitioning in aqueous biphasic systems. *Adv. Colloid Interface Sci.* 239:75–87
12. Banani SF, Lee HO, Hyman AA, Rosen MK. 2017. Biomolecular condensates: organizers of cellular biochemistry. *Nat. Rev. Mol. Cell Biol.* 18:285–98
13. Banani SF, Rice AM, Peeples WB, Lin Y, Jain S, et al. 2016. Compositional control of phase-separated cellular bodies. *Cell* 166:651–63
14. Banerjee PR, Milin AN, Moosa MM, Onuchic PL, Deniz AA. 2017. Reentrant phase transition drives dynamic substructure formation in ribonucleoprotein droplets. *Angew. Chem.* 56:11354–59
15. Banjade S, Rosen MK. 2014. Phase transitions of multivalent proteins can promote clustering of membrane receptors. *eLife* 3:e04123
16. Banjade S, Wu Q, Mittal A, Peeples WB, Pappu RV, Rosen MK. 2015. Conserved interdomain linker promotes phase separation of the multivalent adaptor protein Nck. *PNAS* 112:E6426–35
17. Berry J, Brangwynne CP, Haataja M. 2018. Physical principles of intracellular organization via active and passive phase transitions. *Rep. Prog. Phys.* 81:046601

18. Berry J, Weber SC, Vaidya N, Haataja M, Brangwynne CP. 2015. RNA transcription modulates phase transition-driven nuclear body assembly. *PNAS* 112:E5237–45
19. Bickmore WA. 2013. The spatial organization of the human genome. *Annu. Rev. Genom. Hum. Genet.* 14:67–84
20. Boehning M, Dugast-Darzacq C, Rankovic M, Hansen AS, Yu T, et al. 2018. RNA polymerase II clustering through corboxy-terminal domain phase separation. *Nat. Struct. Mol. Biol.* 25:833–40
21. Boeynaems S, Bogaert E, Kovacs D, Konijnenberg A, Timmerman E, et al. 2017. Phase separation of C9orf72 dipeptide repeats perturbs stress granule dynamics. *Mol. Cell* 65:1044–55.e5
22. Boeynaems S, Holehouse AS, Weinhardt V, Kovacs D, Van Lindt J, et al. 2019. Spontaneous driving forces give rise to protein–RNA condensates with coexisting phases and complex material properties. *PNAS* 116:7889–98
23. Boke E, Ruer M, Wühr M, Coughlin M, Lemaitre R, et al. 2016. Amyloid-like self-assembly of a cellular compartment. *Cell* 166:637–50
24. Bolognesi B, Lorenzo Gotor N, Dhar R, Cirillo D, Baldrighi M, et al. 2016. A concentration-dependent liquid phase separation can cause toxicity upon increased protein expression. *Cell Rep*. 16:222–31
25. Bouchard JJ, Otero JH, Scott DC, Szulc E, Martin EW, et al. 2018. Cancer mutations of the tumor suppressor SPOP disrupt the formation of active, phase-separated compartments. *Mol. Cell* 72:19–36.e8
26. Bracha D, Walls MT, Wei M-T, Zhu L, Kurian M, et al. 2018. Mapping local and global liquid phase behavior in living cells using phto-oligomerizable seeds. *Cell* 175:1467–80.e13
27. Brady JP, Farber PJ, Sekhar A, Lin Y-H, Huang R, et al. 2017. Structural and hydrodynamic properties of an intrinsically disordered region of a germ cell-specific protein on phase separation. *PNAS* 114:E8194–203
28. Brangwynne CP. 2013. Phase transitions and size scaling of membrane-less organelles. *J. Cell Biol.* 203:875–81
29. Brangwynne CP, Eckmann CR, Courson DS, Rybarska A, Hoege C, et al. 2009. Germline P granules are liquid droplets that localize by controlled dissolution/condensation. *Science* 324:1729–32
30. Brangwynne CP, Mitchison TJ, Hyman AA. 2011. Active liquid-like behavior of nucleoli determines their size and shape in *Xenopus laevis* oocytes. *PNAS* 108:4334–39
31. Brangwynne CP, Tompa P, Pappu RV. 2015. Polymer physics of intracellular phase transitions. *Nat. Phys.* 11:899–904
32. Burke KA, Janke AM, Rhine CL, Fawzi NL. 2015. Residue-by-residue view of in vitro FUS granules that bind the C-terminal domain of RNA polymerase II. *Mol. Cell* 60:231–41
33. Burley SK, Petsko GA. 1988. Weakly polar interactions in proteins. *Adv. Protein Chem.* 39:125–89
34. Chen H, Tang AH, Blanpied TA. 2018. Subsynaptic spatial organization as a regulator of synaptic strength and plasticity. *Curr. Opin. Neurobiol.* 51:147–53
35. Choi J-M, Dar F, Pappu RV. 2019. LASSI: a lattice model for simulating phase transitions of multivalent proteins. *PLOS Comput. Biol.* 15:e1007028
36. Cinar H, Cinar S, Chan HS, Winter R. 2018. Pressure-induced dissolution and reentrant formation of condensed, liquid-liquid phase-separated elastomeric α-elastin. *Chemistry* 24:8286–91
37. Courchaine EM, Lu A, Neugebauer KM. 2016. Droplet organelles? *EMBO J.* 35:1603–12
38. Crick SL, Ruff KM, Garai K, Frieden C, Pappu RV. 2013. Unmasking the roles of N- and C-terminal flanking sequences from exon 1 of huntingtin as modulators of polyglutamine aggregation. *PNAS* 110:20075–80
39. Cuylen S, Blaukopf C, Politi AZ, Müller-Reichert T, Neumann B, et al. 2016. Ki-67 acts as a biological surfactant to disperse mitotic chromosomes. *Nature* 535:308–12
40. Dao TP, Kolaitis RM, Kim HJ, O'Donovan K, Martyniak B, et al. 2018. Ubiquitin modulates liquid-liquid phase separation of UBQLN2 via disruption of multivalent interactions. *Mol. Cell* 69:965–78.e6
41. Dao TP, Martyniak B, Canning AJ, Lei Y, Colicino EG, et al. 2019. ALS-linked mutations affect UBQLN2 oligomerization and phase separation in a position- and amino acid-dependent manner. *Structure* 27:937–51.e5
42. Dastidar P. 2019. Designing supramolecular gelators: challenges, frustrations, and hopes. *Gels* 5:15

43. Davey NE, Cyert MS, Moses AM. 2015. Short linear motifs: *ex nihilo* evolution of protein regulation. *Cell Commun. Signaling* 13:43
44. Deshpande S, Brandenburg F, Lau A, Last MGF, Spoelstra WK, et al. 2019. Spatiotemporal control of coacervate formation within liposomes. *Nat. Commun.* 10:1800
45. Dias CS, Araújo NAM, Telo da Gama MM. 2017. Dynamics of network fluids. *Adv. Colloid Interface Sci.* 247:258–63
46. Dignon GL, Zheng W, Kim YC, Best RB, Mittal J. 2018. Sequence determinants of protein phase behavior from a coarse-grained model. *PLOS Comput. Biol.* 14:e1005941
47. Dine E, Gil AA, Uribe G, Brangwynne CP, Toettcher JE. 2018. Protein phase separation provides long-term memory of transient spatial stimuli. *Cell Syst.* 6:655–63.e5
48. Ditlev JA, Case LB, Rosen MK. 2018. Who's in and who's out: compositional control of biomolecular condensates. *J. Mol. Biol.* 430:4666–84
49. Du M, Chen ZJ. 2018. DNA-induced liquid phase condensation of cGAS activates innate immune signaling. *Science* 361:704–9
50. Dzuricky M, Roberts S, Chilkoti A. 2018. Convergence of artificial protein polymers and intrinsically disordered proteins. *Biochemistry* 57:2405–14
51. Elbaum-Garfinkle S, Kim Y, Szczepaniak K, Chen CC-H, Eckmann CR, et al. 2015. The disordered P granule protein LAF-1 drives phase separation into droplets with tunable viscosity and dynamics. *PNAS* 112:7189–94
52. Erdel F, Rippe K. 2018. Formation of chromatin subcompartments by phase separation. *Biophys. J.* 114:2262–70
53. Ermoshkin AV, Olvera de la Cruz M. 2003. A modified random phase approximation of polyelectrolyte solutions. *Macromolecules* 36:7824–32
54. Falahati H, Haji-Akbari A. 2019. Thermodynamically driven assemblies and liquid–liquid phase separations in biology. *Soft Matter* 15:1135–54
55. Falahati H, Wieschaus E. 2017. Independent active and thermodynamic processes govern the nucleolus assembly in vivo. *PNAS* 114:1335–40
56. Fei J, Jadaliha M, Harmon TS, Li IT, Hua B, et al. 2017. Quantitative analysis of multilayer organization of proteins and RNA in nuclear speckles at super resolution. *J. Cell Sci.* 130:4180–92
57. Feric M, Vaidya N, Harmon TS, Mitrea DM, Zhu L, et al. 2016. Coexisting liquid phases underlie nucleolar subcompartments. *Cell* 165:1686–97
58. Flory PJ. 1941. Molecular size distribution in three dimensional polymers. I. Gelation. *J. Am. Chem. Soc.* 63:3083–90
59. Flory PJ. 1942. Thermodynamics of high polymer solutions. *J. Chem. Phys.* 10:51–61
60. Franzmann TM, Jahnel M, Pozniakovsky A, Mahamid J, Holehouse AS, et al. 2018. Phase separation of a yeast prion protein promotes cellular fitness. *Science* 359:eaao5654
61. Freeman Rosenzweig ES, Xu B, Kuhn Cuellar L, Martinez-Sanchez A, Schaffer M, et al. 2017. The eukaryotic CO_2-concentrating organelle is liquid-like and exhibits dynamic reorganization. *Cell* 171:148–62.e19
62. Gasior K, Zhao J, McLaughlin G, Forest MG, Gladfelter AS, Newby J. 2019. Partial demixing of RNA-protein complexes leads to intradroplet patterning in phase-separated biological condensates. *Phys. Rev. E* 99:012411
63. Gomes E, Shorter J. 2019. The molecular language of membraneless organelles. *J. Biol. Chem.* 294:7115–27
64. Han TW, Kato M, Xie S, Wu LC, Mirzaei H, et al. 2012. Cell-free formation of RNA granules: bound RNAs identify features and components of cellular assemblies. *Cell* 149:768–79
65. Harmon TS, Holehouse AS, Pappu RV. 2018. Differential solvation of intrinsically disordered linkers drives the formation of spatially organized droplets in ternary systems of linear multivalent proteins. *New J. Phys.* 20:045002
66. Harmon TS, Holehouse AS, Rosen MK, Pappu RV. 2017. Intrinsically disordered linkers determine the interplay between phase separation and gelation in multivalent proteins. *eLife* 6:e30294

67. Hofweber M, Dormann D. 2019. Friend or foe: post-translational modifications as regulators of phase separation and RNP granule dynamics. *J. Biol. Chem.* 294:7137–50
68. Hofweber M, Hutten S, Bourgeois B, Spreitzer E, Niedner-Boblenz A, et al. 2018. Phase separation of FUS is suppressed by its nuclear import receptor and arginine methylation. *Cell* 173:706–19.e13
69. Honigmann A, Sadeghi S, Keller J, Hell SW, Eggeling C, Vink R. 2014. A lipid bound actin meshwork organizes liquid phase separation in model membranes. *eLife* 3:e01671
70. Hughes MP, Sawaya MR, Boyer DR, Goldschmidt L, Rodriguez JA, et al. 2018. Atomic structures of low-complexity protein segments reveal kinked β sheets that assemble networks. *Science* 359:698–701
71. Huizar RL, Lee C, Boulgakov AA, Horani A, Tu F, et al. 2018. A liquid-like organelle at the root of motile ciliopathy. *eLife* 7:e38497
72. Hyman AA, Weber CA, Jülicher F. 2014. Liquid-liquid phase separation in biology. *Annu. Rev. Cell Dev. Biol.* 30:39–58
73. Jawerth LM, Ijavi M, Ruer M, Saha S, Jahnel M, et al. 2018. Salt-dependent rheology and surface tension of protein condensates using optical traps. *Phys. Rev. Lett.* 121:258101
74. Jenal U, Stephens C. 2002. The Caulobacter cell cycle: timing, spatial organization and checkpoints. *Curr. Opin. Microbiol.* 5:558–63
75. Kato M, Han TW, Xie S, Shi K, Du X, et al. 2012. Cell-free formation of RNA granules: low complexity sequence domains form dynamic fibers within hydrogels. *Cell* 149:753–67
76. Kesten H. 2006. What is. . .percolation? *Not. Am. Math. Soc.* 53:572–73
77. Kim S, Huang J, Lee Y, Dutta S, Yoo HY, et al. 2016. Complexation and coacervation of like-charged polyelectrolytes inspired by mussels. *PNAS* 113:E847–53
78. Kistler KE, Trcek T, Hurd TR, Chen R, Liang FX, et al. 2018. Phase transitioned nuclear Oskar promotes cell division of *Drosophila* primordial germ cells. *eLife* 7:e37949
79. Kroschwald S, Maharana S, Mateju D, Malinovska L, Nüske E, et al. 2015. Promiscuous interactions and protein disaggregases determine the material state of stress-inducible RNP granules. *eLife* 4:e06807
80. Kroschwald S, Munder MC, Maharana S, Franzmann TM, Richter D, et al. 2018. Different material states of Pub1 condensates define distinct modes of stress adaptation and recovery. *Cell Rep.* 23:3327–39
81. Kwon I, Kato M, Xiang S, Wu L, Theodoropoulos P, et al. 2013. Phosphorylation-regulated binding of RNA polymerase II to fibrous polymers of low-complexity domains. *Cell* 155:1049–60
82. Kwon I, Xiang S, Kato M, Wu L, Theodoropoulos P, et al. 2014. Poly-dipeptides encoded by the C9orf72 repeats bind nucleoli, impede RNA biogenesis, and kill cells. *Science* 345:1139–45
83. Langdon EM, Qiu Y, Ghanbari Niaki A, McLaughlin GA, Weidmann CA, et al. 2018. mRNA structure determines specificity of a polyQ-driven phase separation. *Science* 360:922–27
84. Larson AG, Elnatan D, Keenen MM, Trnka MJ, Johnston JB, et al. 2017. Liquid droplet formation by HP1α suggests a role for phase separation in heterochromatin. *Nature* 547:236–40
85. Lee H, DeLoache WC, Dueber JE. 2012. Spatial organization of enzymes for metabolic engineering. *Metab. Eng.* 14:242–51
86. Li HR, Chiang WC, Chou PC, Wang WJ, Huang JR. 2018. TAR DNA-binding protein 43 (TDP-43) liquid–liquid phase separation is mediated by just a few aromatic residues. *J. Biol. Chem.* 293:6090–98
87. Li P, Banjade S, Cheng H-C, Kim S, Chen B, et al. 2012. Phase transitions in the assembly of multivalent signalling proteins. *Nature* 483:336–40
88. Lin Y, Currie SL, Rosen MK. 2017. Intrinsically disordered sequences enable modulation of protein phase separation through distributed tyrosine motifs. *J. Biol. Chem.* 292:19110–20
89. Lin Y, McCarty J, Rauch JN, Delaney KT, Kosik KS, et al. 2019. Narrow equilibrium window for complex coacervation of tau and RNA under cellular conditions. *eLife* 8:e42571
90. Lin Y, Protter DSW, Rosen MK, Parker R. 2015. Formation and maturation of phase-separated liquid droplets by RNA-binding proteins. *Mol. Cell* 60:208–19
91. Lin YH, Chan HS. 2017. Phase separation and single-chain compactness of charged disordered proteins are strongly correlated. *Biophys. J.* 112:2043–46
92. Lin Y-H, Forman-Kay JD, Chan HS. 2016. Sequence-specific polyampholyte phase separation in membraneless organelles. *Phys. Rev. Lett.* 117:178101

93. Linsenmeier M, Kopp MRG, Grigolato F, Emmanoulidis L, Liu D, et al. 2019. Dynamics of synthetic membraneless organelles in microfluidic droplets. *Angew. Chem.* 58:14489–94
94. Low JT, Weeks KM. 2010. SHAPE-directed RNA secondary structure prediction. *Methods* 52:150–58
95. Lu H, Yu D, Hansen AS, Ganguly S, Liu R, et al. 2018. Phase-separation mechanism for C-terminal hyperphosphorylation of RNA polymerase II. *Nature* 558:318–23
96. Maharana S, Wang J, Papadopoulos DK, Richter D, Pozniakovsky A, et al. 2018. RNA buffers the phase separation behavior of prion-like RNA binding proteins. *Science* 360:918–21
97. Mann JR, Gleixner AM, Mauna JC, Gomes E, DeChellis-Marks MR, et al. 2019. RNA binding antagonizes neurotoxic phase transitions of TDP-43. *Neuron* 102:321–38.e8
98. Manz BN, Groves JT. 2010. Spatial organization and signal transduction at intercellular junctions. *Nat. Rev. Mol. Cell Biol.* 11:342–52
99. Mao S, Kuldinow D, Haataja MP, Košmrlj A. 2019. Phase behavior and morphology of multicomponent liquid mixtures. *Soft Matter* 15:1297–311
100. Martin EW, Mittag T. 2018. Relationship of sequence and phase separation in protein low-complexity regions. *Biochemistry* 57:2478–87
101. Marzahn MR, Marada S, Lee J, Nourse A, Kenrick S, et al. 2016. Higher-order oligomerization promotes localization of SPOP to liquid nuclear speckles. *EMBO J.* 35:1254–75
102. Maucuer A, Desforges B, Joshi V, Boca M, Kretov DA, et al. 2018. Microtubules as platforms for probing liquid-liquid phase separation in cells: application to RNA-binding proteins. *J. Cell Sci.* 131:jcs214692
103. McCarty J, Delaney KT, Danielsen SPO, Fredrickson GH, Shea J-E. 2019. Complete phase diagram for liquid–liquid phase separation of intrinsically disordered proteins. *J. Phys. Chem. Lett.* 10:1644–52
104. McGurk L, Gomes E, Guo L, Mojsilovic-Petrovic J, Tran V, et al. 2018. Poly(ADP-ribose) prevents pathological phase separation of TDP-43 by promoting liquid demixing and stress granule localization. *Mol. Cell* 71:703–17.e9
105. Milles S, Salvi N, Blackledge M, Jensen MR. 2018. Characterization of intrinsically disordered proteins and their dynamic complexes: from in vitro to cell-like environments. *Prog. Nucl. Magn. Reson. Spectrosc.* 109:79–100
106. Milovanovic D, De Camilli P. 2017. Synaptic vesicle clusters at synapses: a distinct liquid phase? *Neuron* 93:995–1002
107. Milovanovic D, Wu Y, Bian X, De Camilli P. 2018. A liquid phase of synapsin and lipid vesicles. *Science* 361:604–7
108. Mitrea DM, Cika JA, Guy CS, Ban D, Banerjee PR, et al. 2016. Nucleophosmin integrates within the nucleolus via multi-modal interactions with proteins displaying R-rich linear motifs and rRNA. *eLife* 5:e13571
109. Mitrea DM, Cika JA, Stanley CB, Nourse A, Onuchic PL, et al. 2018. Self-interaction of NPM1 modulates multiple mechanisms of liquid–liquid phase separation. *Nat. Commun.* 9:842
110. Mitrea DM, Grace CR, Buljan M, Yun M-K, Pytel NJ, et al. 2014. Structural polymorphism in the N-terminal oligomerization domain of NPM1. *PNAS* 111:4466–71
111. Mitrea DM, Kriwacki RW. 2016. Phase separation in biology: functional organization of a higher order. *Cell Commun. Signal.* 14:1
112. Molliex A, Temirov J, Lee J, Coughlin M, Kanagaraj AP, et al. 2015. Phase separation by low complexity domains promotes stress granule assembly and drives pathological fibrillization. *Cell* 163:123–33
113. Monahan Z, Ryan VH, Janke AM, Burke KA, Rhoads SN, et al. 2017. Phosphorylation of the FUS low-complexity domain disrupts phase separation, aggregation, and toxicity. *EMBO J.* 36:2951–67
114. Monterroso B, Zorrilla S, Sobrinos-Sanguino M, Keating CD, Rivas G. 2016. Microenvironments created by liquid-liquid phase transition control the dynamic distribution of bacterial division FtsZ protein. *Sci. Rep.* 6:35140
115. Monterroso B, Zorrilla S, Sobrinos-Sanguino M, Robles-Ramos MA, López-Álvarez M, et al. 2019. Bacterial FtsZ protein forms phase-separated condensates with its nucleoid-associated inhibitor SlmA. *EMBO Rep.* 20:e45946
116. Muiznieks LD, Cirulis JT, van der Horst A, Reinhardt DP, Wuite GJ, et al. 2014. Modulated growth, stability and interactions of liquid-like coacervate assemblies of elastin. *Matrix Biol.* 36:39–50

117. Nguemaha V, Zhou HX. 2018. Liquid-liquid phase separation of patchy particles illuminates diverse effects of regulatory components on protein droplet formation. *Sci. Rep.* 8:6728
118. Niewidok B, Igaev M, Pereira da Graca A, Strassner A, Lenzen C, et al. 2018. Single-molecule imaging reveals dynamic biphasic partition of RNA-binding proteins in stress granules. *J. Cell Biol.* 217:1303–18
119. Nikolic J, Le Bars R, Lama Z, Scrima N, Lagaudrière-Gesbert C, et al. 2017. Negri bodies are viral factories with properties of liquid organelles. *Nat. Commun.* 8:58
120. Nott TJ, Craggs TD, Baldwin AJ. 2016. Membraneless organelles can melt nucleic acid duplexes and act as biomolecular filters. *Nat. Chem.* 8:569–75
121. Nott TJ, Petsalaki E, Farber P, Jervis D, Fussner E, et al. 2015. Phase transition of a disordered nuage protein generates environmentally responsive membraneless organelles. *Mol. Cell* 57:936–47
122. Orlando G, Raimondi D, Tabaro F, Codice F, Moreau Y, Vranken W. 2019. Computational identification of prion-like RNA-binding proteins that form liquid phase-separated condensates. *Bioinformatics* 35:4617–23
123. Pak CW, Kosno M, Holehouse AS, Padrick SB, Mittal A, et al. 2016. Sequence determinants of intracellular phase separation by complex coacervation of a disordered protein. *Mol. Cell* 63:72–85
124. Pappu RV, Wang X, Vitalis A, Crick SL. 2008. A polymer physics perspective on driving forces and mechanisms for protein aggregation. *Arch. Biochem. Biophys.* 469:132–41
125. Papusheva E, Heisenberg CP. 2010. Spatial organization of adhesion: force-dependent regulation and function in tissue morphogenesis. *EMBO J.* 29:2753–68
126. Patel A, Lee HO, Jawerth L, Maharana S, Jahnel M, et al. 2015. A liquid-to-solid phase transition of the ALS protein FUS accelerated by disease mutation. *Cell* 162:1066–77
127. Patel A, Malinovska L, Saha S, Wang J, Alberti S, et al. 2017. ATP as a biological hydrotrope. *Science* 356:753–56
128. Petsev DN, Wu X, Galkin O, Vekilov PG. 2003. Thermodynamic functions of concentrated protein solutions from phase equilibria. *J. Phys. Chem. B* 107:3921–26
129. Pierce WK, Grace CR, Lee J, Nourse A, Marzahn MR, et al. 2016. Multiple weak linear motifs enhance recruitment and processivity in SPOP-mediated substrate ubiquitination. *J. Mol. Biol.* 428:1256–71
130. Pliss A, Levchenko SM, Liu L, Peng X, Ohulchanskyy TY, et al. 2019. Cycles of protein condensation and discharge in nuclear organelles studied by fluorescence lifetime imaging. *Nat. Commun.* 10:455
131. Posey AE, Ruff KM, Harmon TS, Crick SL, Li A, et al. 2018. Profilin reduces aggregation and phases separation of huntingtin N-terminal fragments by preferentially binding to soluble monomers and oligomers. *J. Biol. Chem.* 293:3734–46
132. Powers SK, Holehouse AS, Korasick DA, Schreiber KH, Clark NM, et al. 2019. Nucleo-cytoplasmic partitioning of ARF proteins controls auxin responses in *Arabidopsis thaliana*. *Mol. Cell* 76:177–90.e5
133. Protter DSW, Parker R. 2016. Principles and properties of stress granules. *Trends Cell Biol.* 26:668–79
134. Prusty D, Pryamitsyn V, Olvera de la Cruz M. 2018. Thermodynamics of associative polymer blends. *Macromolecules* 51:5918–32
135. Putnam A, Cassani M, Smith J, Seydoux G. 2019. A gel phase promotes condensation of liquid P granules in *Caenorhabditis elegans* embryos. *Nat. Struct. Mol. Biol.* 26:220–26
136. Rai AK, Chen JX, Selbach M, Pelkmans L. 2018. Kinase-controlled phase transition of membraneless organelles in mitosis. *Nature* 559:211–16
137. Rao BS, Parker R. 2017. Numerous interactions act redundantly to assemble a tunable size of P bodies *Saccharomyces cerevisiae*. *PNAS* 114:E9569–78
138. Razin SV, Gavrilov AA, Yarovaya OV. 2010. Transcription factories and spatial organization of eukaryotic genomes. *Biochem. Biokhim.* 75:1307–15
139. Riback JA, Katanski CD, Kear-Scott JL, Pilipenko EV, Rojek AE, et al. 2017. Stress-triggered phase separation is an adaptive, evolutionarily tuned response. *Cell* 168:1028–40.e19
140. Riback JA, Zhu L, Ferrolino MC, Tolbert M, Mitrea DM, et al. 2019. Composition dependent phase separation underlies directional flux through the nucleolus. bioRxiv 809210. **https://doi.org/10.1101/809210**
141. Roberts S, Harmon TS, Schaal JL, Miao V, Li K, et al. 2018. Injectable tissue integrating networks from recombinant polypeptides with tunable order. *Nat. Mater.* 17:1154–63

142. Rubinstein M, Colby RH. 2003. *Polymer Physics*. Oxford, UK: Oxford Univ. Press
143. Rubinstein M, Dobrynin AV. 1997. Solutions of associative polymers. *Trends Polymer Sci.* 5:181–86
144. Ruff KM, Harmon TS, Pappu RV. 2015. CAMELOT: a machine learning approach for coarse-grained simulations of aggregation of block-copolymeric protein sequences. *J. Chem. Phys.* 143:243123
145. Sabari BR, Dall'Agnese A, Boija A, Klein IA, Coffey EL, et al. 2018. Coactivator condensation at super-enhancers links phase separation and gene control. *Science* 361:eaar3958
146. Saito M, Hess D, Eglinger J, Fritsch AW, Kreysing M, et al. 2019. Acetylation of intrinsically disordered regions regulates phase separation. *Nat. Chem. Biol.* 15:51–61
147. Salvi N, Abyzov A, Blackledge M. 2017. Atomic resolution conformational dynamics of intrinsically disordered proteins from NMR spin relaxation. *Prog. Nucl. Magn. Reson. Spectrosc.* 102–103:43–60
148. Šarić A, Buell AK, Meisl G, Michaels TCT, Dobson CM, et al. 2016. Physical determinants of the self-replication of protein fibrils. *Nat. Phys.* 12:874–80
149. Sarkar J, Myong S. 2018. Single-molecule and ensemble methods to probe initial stages of RNP granule assembly. *Methods Mol. Biol.* 1814:325–38
150. Schuster BS, Reed EH, Parthasarathy R, Jahnke CN, Caldwell RM, et al. 2018. Controllable protein phase separation and modular recruitment to form responsive membraneless organelles. *Nat. Commun.* 9:2985
151. Semenov AN, Rubinstein M. 1998. Thermoreversible gelation in solutions of associative polymers. 1. Statics. *Macromolecules* 31:1373–85
152. Shan Z, Tu Y, Yang Y, Liu Z, Zeng M, et al. 2018. Basal condensation of Numb and Pon complex via phase transition during *Drosophila* neuroblast asymmetric division. *Nat. Commun.* 9:737
153. Shin Y, Berry J, Pannucci N, Haataja MP, Toettcher JE, Brangwynne CP. 2017. Spatiotemporal control of intracellular phase transitions using light-activated optoDroplets. *Cell* 168:159–71.e14
154. Shin Y, Brangwynne CP. 2017. Liquid phase condensation in cell physiology and disease. *Science* 357:eaaf4382
155. Simon JR, Carroll NJ, Rubinstein M, Chilkoti A, López GP. 2017. Programming molecular self-assembly of intrinsically disordered proteins containing sequences of low complexity. *Nat. Chem.* 9:509–15
156. Sommer J-U. 2018. Gluonic and regulatory solvents: a paradigm for tunable phase segregation in polymers. *Macromolecules* 51:3066–74
157. Stanek D, Fox AH. 2017. Nuclear bodies: news insights into structure and function. *Curr. Opin. Cell Biol.* 46:94–101
158. Stockmayer WH. 1943. Theory of molecular size distribution and gel formation in branched-chain polymers. *J. Chem. Phys.* 11:45–55
159. Strom AR, Emelyanov AV, Mir M, Fyodorov DV, Darzacq X, Karpen GH. 2017. Phase separation drives heterochromatin domain formation. *Nature* 547:241–45
160. Su X, Ditlev JA, Hui E, Xing W, Banjade S, et al. 2016. Phase separation of signaling molecules promotes T cell receptor signal transduction. *Science* 352:595–99
161. Tang SJ. 2017. Potential role of phase separation of repetitive DNA in chromosomal organization. *Genes* 8:279
162. Taylor JP, Brown RH Jr., Cleveland DW. 2016. Decoding ALS: from genes to mechanism. *Nature* 539:197–206
163. Taylor NO, Wei M-T, Stone HA, Brangwynne CP. 2019. Quantifying dynamics in phase-separated condensates using fluorescence recovery after photobleaching. *Biophys. J.* 117:1285–300
164. Ukmar-Godec T, Hutten S, Grieshop MP, Rezaei-Ghaleh N, Cima-Omori MS, et al. 2019. Lysine/RNA-interactions drive and regulate biomolecular condensation. *Nat. Commun.* 10:2909
165. Vekilov PG. 2010. Phase transitions of folded proteins. *Soft Matter* 6:5254–72
166. Vernon RM, Chong PA, Tsang B, Kim TH, Bah A, et al. 2018. Pi-Pi contacts are an overlooked protein feature relevant to phase separation. *eLife* 7:e31486
167. Vernon RM, Forman-Kay JD. 2019. First-generation predictors of biological protein phase separation. *Curr. Opin. Struct. Biol.* 58:88–96
168. Walter H, Brooks DE. 1995. Phase separation in cytoplasm, due to macromolecular crowding, is the basis for microcompartmentation. *FEBS Lett.* 361:135–39

169. Wang H, Yan X, Aigner H, Bracher A, Nguyen ND, et al. 2019. Rubisco condensate formation by CcmM in β-carboxysome biogenesis. *Nature* 566:131–35
170. Wang J, Choi J-M, Holehouse AS, Lee HO, Zhang X, et al. 2018. A molecular grammar governing the driving forces for phase separation of prion-like RNA binding proteins. *Cell* 174:688–99.e16
171. Wang N, Liu C. 2019. Implications of liquid-liquid phase separation in plant chromatin organization and transcriptional control. *Curr. Opin. Genet. Dev.* 55:59–65
172. Wang Z, Zhang H. 2019. Phase separation, transition, and autophagic degradation of proteins in development and pathogenesis. *Trends Cell Biol.* 29:417–27
173. Wei MT, Elbaum-Garfinkle S, Holehouse AS, Chen CC, Feric M, et al. 2017. Phase behaviour of disordered proteins underlying low density and high permeability of liquid organelles. *Nat. Chem.* 9:1118–25
174. Weirich KL, Banerjee S, Dasbiswas K, Witten TA, Vaikuntanathan S, Gardel ML. 2017. Liquid behavior of cross-linked actin bundles. *PNAS* 114:2131–36
175. Wheeler JR, Matheny T, Jain S, Abrisch R, Parker R. 2016. Distinct stages in stress granule assembly and disassembly. *eLife* 5:e18413
176. Woodruff JB. 2018. Assembly of mitotic structures through phase separation. *J. Mol. Biol.* 430:4762–72
177. Woodruff JB, Ferreira Gomes B, Widlund PO, Mahamid J, Honigmann A, Hyman AA. 2017. The centrosome is a selective condensate that nucleates microtubules by concentrating tubulin. *Cell* 169:1066–77.e10
178. Wu H, Fuxreiter M. 2016. The structure and dynamics of higher-order assemblies: amyloids, signalosomes, and granules. *Cell* 165:1055–66
179. Wu X, Cai Q, Shen Z, Chen X, Zeng M, et al. 2019. RIM and RIM-BP form presynaptic active-zone-like condensates via phase separation. *Mol. Cell* 73:971–84.e5
180. Wunder T, Cheng SLH, Lai SK, Li HY, Mueller-Cajar O. 2018. The phase separation underlying the pyrenoid-based microalgal Rubisco supercharger. *Nat. Commun.* 9:5076
181. Yang Y, Jones HB, Dao TP, Castañeda CA. 2019. Single amino acid substitutions in stickers, but not spacers, substantially alter UBQLN2 phase transitions and dense phase material properties. *J. Phys. Chem. B* 123:3618–29
182. Yoo H, Triandafillou C, Drummond DA. 2019. Cellular sensing by phase separation: using the process, not just the products. *J. Biol. Chem.* 294:7151–59
183. Zhang H, Elbaum-Garfinkle S, Langdon EM, Taylor N, Occhipinti P, et al. 2015. RNA controls polyQ protein phase transitions. *Mol. Cell* 60:220–30
184. Zhou HX, Nguemaha V, Mazarakos K, Qin S. 2018. Why do disordered and structured proteins behave differently in phase separation? *Trends Biochem. Sci.* 43:499–516
185. Zwanzig R, Mountain RD. 1965. High-frequency elastic moduli of simple fluids. *J. Chem. Phys.* 43:4464–71
186. Zwicker D, Decker M, Jaensch S, Hyman AA, Jülicher F. 2014. Centrosomes are autocatalytic droplets of pericentriolar material organized by centrioles. *PNAS* 111:E2636–45